Atypical Cadherin FAT3 Is a Novel Mediator for Morphological Changes of Microglia

January 2020

Tomomi OKAJIMA

Atypical Cadherin FAT3 Is a Novel Mediator for Morphological Changes of Microglia

A Dissertation Submitted to
the Graduate School of Life and Environmental Sciences,
the University of Tsukuba in Partial Fulfillment of the Requirements
for the Degree of Doctor of Philosophy in Science
(Doctoral Program in Biological Sciences)

Tomomi OKAJIMA

TABLE OF CONTENTS

ABSTRACT

Microglia are resident macrophages, which are critical for brain development and homeostasis. Microglial morphology is dynamically changed during postnatal stages, leading to regulating neural circuit formation, including neurogenesis, synaptogenesis, and synapse pruning. The functional transition in microglia has been considered to correlate with their morphological changes over time. In previous research, it has been well known that the shape of microglia is also altered in response to the detritus of the apoptotic cells and pathogens such as bacteria and viruses. Although the morphological changes are crucial for acquiring microglial functions, the morphological changes of microglia during juvenile rather than adults are not fully understood. Here I report that an atypical cadherin family protein, FAT3, regulates microglial morphology by contributing to the stabilization of microglial projections. I found that the shape of mouse microglia cell line BV2 becomes elongated in a high nutrient medium. Using microarray analysis, I identified that FAT3 expression is induced by culturing at high nutrient medium. Knockdown of FAT3 increased the number of round shapes and shortens the time of sustaining the elongation forms. Moreover, I found that purinergic analog, hypoxanthine, promotes FAT3 expression and morphological changes in BV2. Additionally, the microglial ramifications and synapse pruning are enhanced in FAT3 deficient mice. These data suggest that the FAT3 expression associated with hypoxanthine is a novel pathway associated with microglial morphology and functions. My data provide a possibility that microglial FAT3 control brain homeostasis via regulation of microglial morphology and functions *in vivo*.

INTRODUCTION

Microglia play important roles in regulating not only the immune system but also neural circuit construction in the central nervous systems (Kettenmann et al., 2011). Previous study has reported that microglia exhibit the amoeboid shape during prenatal birth and gradually transform into ramified shape by postnatal day (P) 14. Usually, amoeboid microglia are thought to be reactive forms, which possess a high ability for engulfment. Because neuronal cell deaths frequently occur during the developmental stages, reactive microglia eliminate the apoptotic or vulnerable neurons to regulate the number of neurons and brain environments (Marin-Teva et al., 2004) (Cunningham et al., 2013). On the other hand, microglia have been known to regulate neural circuit formation during the postnatal brain. The proper neural circuit formation is regulated by a variety of neuronal events, such as neuronal survival, apoptosis, synaptogenesis, and synapse pruning (Marin-Teva et al., 2004) (Sierra et al., 2010) (Paolicelli et al., 2011) (Cunningham et al., 2013) (Ueno et al., 2013) (Miyamoto et al., 2016). In particular, the control of synaptic connectivity is a key process that underlies the higher brain functions. Previous studies have shown that the number of synapses is dramatically increased during brain development, followed by reducing them by microglia (Lichtman and Colman, 2000). In the case of normal development in mice, the synaptic pruning approximately occurs from P20 to P30. At this time, microglial morphology exhibits the ramified shape, which is a surveillance type. This type of microglia constantly elongates and retracts their processes to monitor the neural circuit even in the resting state (Nimmerjahn et al., 2005) (Haynes et al., 2006). Microglia contribute to the proper neural circuit formation by removing unnecessary synapses (Paolicelli et al., 2011) (Schafer et al., 2012). It is thought that a set of these morphological alterations in microglia is tightly regulated not only by genetic programs but also by various factors, such as metabolites and exogenous factors, followed by constructing precise neural circuit and maintaining normal brain homeostasis. Although the morphological changes of microglia are implicated in their activity, the cues that modulate microglial morphology, particularly the intrinsic substances, have not been fully explicated.

Microglia is important for synaptogenesis in developmental stages. It is known that developmental neurons produce excessive synapses as a system to promote normal neural circuit formation(Hua and Smith, 2004). For the development of properly connected neural circuits, overproduced synapses require the elimination of overproduced synapses and the maintenance of connections. Microglia-mediated synaptic pruning and formations are processes that occurs in various

brain regions during development (Miyamoto et al., 2016). The complement receptor CR3 and the phagocytic receptor TREM2 receptors expressed in microglia are known to be involved as a mechanism for pruning immature synapses (Stevens et al., 2007) (Schafer et al., 2012) (Filipello et al., 2018). Microglia recognize the expression of C1q and C3 in neurons (the "Eat me" signal) and thus prune the synapses. In contrast, it has also reported that the mechanism by which microglia presented with CD47 from neurons evade synaptic pruning (called “Don’t eat me” signaling) (Lehrman et al., 2018). However, the full picture of the mechanism by which microglia regulate synaptic pruning is still unclear.

The cadherin family proteins play an important role in brain development, synapse connectivity, and neural circuit formation (Takeichi, 2007). In addition, mutations in cadherin family genes cause psychiatric and developmental disorders, including schizophrenia and autism spectrum disorder (ASD) (Redies et al., 2012). Thus, cadherin proteins in the brain are crucial for acquiring proper brain functions. So far, several groups have reported that atypical cadherins are expressed in the central nervous system and tightly regulate brain development. FAT3, which is one of the four FAT-related genes (Fat1-Fat4), is known to be abundantly expressed in the mammalian brain (Nagae et al., 2007) (Zhang et al., 2014). Fat3 gene encodes the transmembrane proteins that possess large extracellular domains and is an ortholog of the Drosophila fat-like gene. In Drosophila, Fat-like induces aberrant actin filament orientation in the ovary (Viktorinova et al., 2009). In the central nervous system, FAT3 is mostly expressed in neurons and regulates neuronal morphology in the retina (Deans et al., 2011) (Krol et al., 2016). On the other hand, the functions of FAT3 in microglia have not been elucidated although FAT3 is expressed in microglia during the postnatal stage (Bennett et al., 2016).

Recent studies have reported that purinergic signaling plays important role in regulating aspects of microglia under brain development (Fields and Burnstock, 2006). Purine derivatives, including ATP and ADP, are released from cells to the extracellular region and activate microglia via purinergic receptors crucial for various physiological processes in the central nervous system. Hypoxanthine, one of the purine derivatives, is implicated in brain development under the postnatal stage. For instance, newborns of mammals are exposed to hypoxic conditions at the time of birth and hypoxanthine may become a marker of hypoxia. Indeed, abnormal hypoxic conditions trigger aberrant brain development (Saugstad, 1988). Moreover, it is known that perturbed hypoxanthine concentration

is tightly associated with ASD (Gevi et al., 2016). Thus, precise regulation of purine derivatives, such as hypoxanthine, is essential for the normal brain establishment.

In this study, I found that the expression of atypical cadherin, FAT3, alters the morphology of microglia BV2 cells. Moreover, hypoxanthine induces FAT3 expression associated with their morphology. My data provide the first evidence that links nucleic acid metabolism in microglia to their morphological regulation.

MATERIALS AND METHODS

Cell culture and stimulation

BV2 cells were cultured in either Dulbecco's Modified Eagle Medium (High Glucose) (DMEM) (Wako, Osaka, Japan) or DMEM/Nutrient Mixture F-12 (DMEM/F12) (Thermo Fisher, Waltham, MA, U.S.) containing 10% fetal bovine serum (FBS), 100 units penicillin and 100 mg streptomycin (P/S) (Thermo Fisher). For screening, BV2 cells were cultured in DMEM with 10% FBS and P/S in the presence or absence of 150 μM L-Alanine (Wako), 50 μM L-Glutamic acid (Wako), 50 μM L-Aspartic acid (Wako), 50 μM L-Asparagine (Wako), 150 μM L-Proline (Wako), 0.0052 pM $CuSO_4$ (Wako), 1.5 pM $FeSO_4$ (Wako), 1.5 pM $ZnSO_4$ (Wako), 150 nM Linoleic acid (Wako), 500 nM Lipoic acid (SIGMA, St. Louis, MO, U.S.), 15 nM Biotin (SIGMA), 500 nM Vitamin B12 (Wako), and 15 μM Hypoxanthine (SIGMA). PPADS was purchased from Alexis Corporation (Lausen, Switzerland). Dipyridamole and Allopurinol were purchased from Tokyo Chemical Industry (Tokyo, Japan). Hoechst 33342 was purchased from Thermo Fisher. DAPI was purchased from Dojindo (Kumamoto, Japan). FAT3 siRNAs (NM_001080814, siRNA ID; SASI_Mm02_00293873) (SIGMA) and MISSION siRNA universal negative control (SIC001) (SIGMA) were purchased from SIGMA. 50 nM FAT3 siRNAs were transfected using Lipofectamine RNAi Max Reagent (Thermo Fisher) according to the manufacturer's instructions.

Plasmid construction and antibody

A cDNA fragment encoding a C-terminus of human-FAT3 containing 276 residues (4313 - 4589 amino acid) was amplified from FAT3 cDNA (Product ID; ORK04991) (Kazusa, Chiba, Japan) and subcloned into the *Bam*HI site of pET28(a) and the *Bgl*II site of pCS4-HA. The primers used were as follows:

FAT3_HA forward, 5'-AAGGATCCGCCACCCGCAAGAAGGTCTTCCGC-3';

FAT3_HA reverse, 5'-CCGGATCCCTACACTTGAGTCTGATGCTGAGTCTCCAC-3';

FAT3_recombinant forward, 5' AAGGATCCGCCACCCGCAAGAAGGTCTTCAGAAAG 3';

FAT3_recombinant reverse, 5' AAGGATCCCTACACCTGGGTCTGCTGCTGTG 3'.

His-tagged recombinant protein was produced in *Escherichia coli* BL21. The His-tagged FAT3 recombinant protein was purified using a Ni-Sepharose 6 Fast Flow (GE Healthcare, Chicago, IL, U.S.), emulsified with Freund’s complete and incomplete adjuvant (Difco Laboratories, Detroit, MI, U.S.), and were injected intradermally into female New Zealand white rabbits (Kitayama Labes,

Nagano, Japan). The FAT3 antibodies were purified by fractionation with ammonium sulfate (0 - 40% saturation), followed by immunoaffinity chromatography on a CNBr-activated Sepharose 4B (GE Healthcare) column that had been conjugated with GST-fused FAT3-C protein carrying the C-terminal 276-residues sequence. FAT3-C antibody was concentrated 5x with a Vivaspin-100K (GE Healthcare). For immunoblot analyses, anti-HA (3F10, Roche, Basel, Switzerland) and anti-Tubulin (DM1A, SIGMA) antibodies were used as primary antibodies.

RT-qPCR

BV-2 cells (1.5 x 10^5 cells/dish in 60mm dish) were cultured for 24 hours at 37 ℃ with 5% CO_2. The cells were treated with various stimulations for 24 hours at 37 ℃ with 5% CO_2. Total RNAs from cells were isolated by ISOGEN II (NIPPON GENE, Tokyo, Japan) according to the manufacturer's instructions. The cDNAs were synthesized by reverse transcriptase, 100 units ReverTra Ace (TOYOBO, Osaka, Japan) together with 25 pmol Random Primer (nonamer) (TOYOBO), 20 nmol dNTPs and 1.0 μg total RNAs. The qPCR was performed in triplicate in 96-well plates (Thermo Fisher) using THUNDERBIRD SYBR qPCR Mix (TOYOBO) in Thermal Cycler Dice Real Time System TP800 (TAKARA, Shiga, Japan) or Applied Biosystems 7900HT Fast Real Time PCR System (Applied Biosystems, Waltham, MA, U.S.). The relative quantity of the target expression was calculated by 2-ΔΔCt methods using Thermal Cycler Dice Real Time System Software (TAKARA) or SDS Software 2.4.2 (Applied Biosystems) with the following calculation. The relative quantity = 2-ΔΔCt, ΔΔCt = (Ct target - Ct 5S) sample - (Ct target - Ct 5S) reference, Ct; Threshold Cycle.

The primers used were as follows:

FAT3 forward, 5'-TATAGGAACGTGCGCTGCACCTGTAATG-3';

FAT3 reverse, 5'-TCATAGCCCACACATTGCATGTCCTCTG-3';

5S rRNA forward, 5'-CGGCCATACCACCCTGAAC-3';

5S rRNA reverse, 5'-GCGGTCTCCCATCCAAGTAC-3';

Morphological assay

BV2 cells were plated at 5.0 x 10^4 cells/dish in a 35mm dish under DMEM/F12, allowed to settle for 24 hours at 37 ℃ with 5% CO_2. Following the plating, BV-2 cells changed the medium to fresh DMEM and DMEM/F12 and incubated for 24 hours at 37 ℃ with 5% CO_2. The images were collected by use of on BIOREVO BZ-9000 (Keyence, Osaka, Japan) equipped with 20x S Plan Fluor

0.45NA (Nikon, Tokyo, Japan) objective lenses controlled by BZ-II software (Keyence). Cells were traced by FIJI image J software and quantified Feret diameters as a parameter of morphology. To quantify the morphology, I took the 5 to 10 fields of view (20,2609 μm2/field). The elongated cells were defined by a Feret diameter score higher than or equal to 2. The number of samples in each experiment are given in Extended Data Table 2.

Immunoblot analysis

HEK293T cells were plated 5.0 x 10^5 cells on 6 well plate and incubated at 5% CO_2 and 37 ºC for one day. Cells were transfected using polyethyleneimine MAX (Polyscience, Warrington, PA, U.S.) and collected with lysis buffer (20 mM Tris-HCl (pH 8.0), 150 mM NaCl, 1 mM EDTA, 0.5% NP-40, 1 mM DTT). Cell lysates were centrifuged at 14,000 r.p.m for 5 minutes. The supernatant was run on SDS-PAGE for protein separation, followed by electrophoretic transfer to a polyvinylidene difluoride membrane. After 1 hour blocking at room temperature, membranes were incubated with primary antibodies for overnight at 4°C. The proteins on membrane were then detected with HRP-conjugated secondary antibodies and chemiluminescence reagent (Amersham ECL Prime Western Blotting Detection Reagents (GE Healthcare) or Chemi-Lumi One Super (Nacarai tesque, Kyoto, Japan).

Immunocytochemistry

0.5 x 10^5 BV2 cells were plated on 15 mm coverslips and grown in 12-well plates in each condition. The cells were fixed with 4% paraformaldehyde (Merck KGaA, Darmstadt, Germany) in phosphate-buffered saline (PBS) for 10 minutes at room temperature. The coverslips were washed in PBS, blocked with 5% bovine serum albumin (BSA) (Wako) in PBS with 0.4% Triton X-100 (MP Biomedicals, Santa Ana, CA, U.S.), then incubated with the FAT3 antibody (1:250) for overnight at 4°C. Following PBS wash, samples were incubated with the secondary antibody; Alexa Fluor 488 anti-rabbit IgG (1:500) (Thermo Fisher) for 30 minutes at room temperature in blocking solution. Cells were imaged using a confocal laser scanning fluorescence microscopy (LSM700) (Carl Zeiss, Oberkochen, Germany) and BIOREVO BZ-9000 (Keyence).

Microarray analysis

3.0 x 10^5 BV2 cells were plated on a 60 mm dish in the DMEM/F12 and replaced cells with either DMEM or DMEM/F12 on the next day. After one day incubation, total RNAs were extracted from

each cell using ISOGEN II (NIPPON GENE) according to the manufacturer's instructions. The single-stranded cDNAs were generated from total RNA (100 ng) using Ambion WT Expression kit (Ambion Inc, Austin, TX, U.S.), sequentially fragmented and covalently linked to biotin using GeneChip WT Terminal Labeling and Hybridization kit (Affymetrix, Santa Clara, CA, U.S.) according to the manufacturer's instructions. These samples were incubated at 45°C at 60 rpm for 17 hours to hybridize on Affymetrix GeneChip Mouse Gene 1.0 ST arrays. After hybridization, each probe array was washed and stained with Affymetrix GeneChip Fluidics Station 450 and scanned by Affymetrix GeneChip Scanner 3000. Data were analyzed with Affymetrix Expression Console software and Affymetrix Transcriptome Analysis Console. The GEO accession numbers for the array dataset are GSM4306479 and GSM4306480.

Hypoxanthine measurement assay

1.0×10^6 BV2 cells were incubated on a 100 mm dish in the DMEM together with 15 μM hypoxanthine. After 12 hours, cells were treated with 10 μM dipyridamole or 10 μM allopurinol for 3 hours. BV2 cells were incubated with ice cold xanthine assay buffer (BioVison, Milpitas, CA, U.S.) for 10 min on ice. Cells were collected by scraper and subjected to hypoxanthine measurement assay according to the manufacturer's instructions of the Xanthine/Hypoxanthine Colorimetric/Fluorometric Assay Kit (BioVision, Milpitas, CA, U.S.).

Live cell imaging analysis

BV2 cells were plated 1.0 x 105 cells in a 35 mm dish and incubated for 24 hours. Media were replaced with DMEM containing 1.0 ng/μL Lipopolysaccharide (LPS) in the presence or absence of 15 μM hypoxanthine and were then subjected to the imaging analysis. Live cell imagings were conducted on BIOREVO BZ-9000 (Keyence, Osaka, Japan) equipped with 20x S Plan Fluor 0.45NA (Nikon, Tokyo, Japan) objective lenses controlled by BZ-II software (Keyence). BV2 cells were imaged at one frame per 15 minutes for 12 hours. The images were analyzed using FIJI image J software. Briefly, the Feret's diameter in each cell was quantified using the function of Set Measurements in Fiji ImageJ. The elongated cells were defined by a Feret diameter score higher than or equal to 3.

Primary culture of microglia

The monoclonal CD11b antibody is generated using the M1/70 hybridoma cell line

(M1/70.15.11.5.2-f, Developmental Studies Hybridoma Bank, The University of Iowa, Iowa City, IA, U.S.) grown in Hybridoma-SFM (Thermo Fisher). The medium containing CD11b antibody was collected by centrifugation when cells were grown until confluent. One day before mice dissection, the sterile Petri dishes were incubated in a solution of 50 mM Tris-HCl (pH9.5) with 6 mg/mL goat-anti-mouse IgG secondary antibody (Jackson ImmunoResearch, West Grove, PA, U.S.) for 1 hour at 37 ℃. The dishes were rinsed with PBS three times and CD11b antibody was added to 10 mm Petri dishes for overnight at 37 ℃ 5% CO^2 followed by washing the Petri dishes. ICR pups (P1 to P3) (SLC, Shizuoka, Japan) were rapidly dissected and placed into ice-cold PBS. The brains were chopped with a scalpel blade and surgical scissors. The tissues were suspended in 5 mL of ice-cold PBS containing 40 units DNaseI (Wako) and were transferred to a Dounce homogenizer equipped with a loose pestle (DWK Life Sciences GmbH, Wertheim, Germany) The tissues were homogenized 10 times by gentle and incomplete strokes and were centrifuged at 500 x g for 15 min at 4 ℃. After discarding the supernatant, cell pellets were resuspended in 5 ml of PBS containing 2 mg/mL peptone from milk solids (Sigma), passed through a 70 μm cell strainer (BD Biosciences, Bedford, MA, USA), and applied directly to positive selection immunopanning dishes coated with CD11b antibodies. Cells were incubated for 20 min at room temperature. Unattached cells and debris were removed by washing with PBS without Ca^{2+} and Mg^{2+} ten times.

The attached cells to the immunopanning dishes were treated with 0.25 % trypsin/1 mM EDTA for 1 min at 37 ℃ with 5 % CO^2 and the cells were recovered by repeated pipetting with 4 mL of DMEM. The recovered cells were centrifuged at 500 x g for 15 min at 4 ℃ and the supernatant was removed with 1mL of the medium and resuspended with cells gently. For immunocytochemistry, 15 μl drop of Bovine Collagen Coating Solution (CELL applications, San Diego, CA, USA) in the center of coverslips in 24-well culture plate and incubate for 15 min at 37 ℃ with 5 % CO^2. After aspirating the collagen spot, the suspended cells were immediately plated at 3.5 x 10^3 cells/spot for 10 min at 37 ℃ with 5 % CO^2. The attached cells were incubated under 500 μL of either DMEM, DMEM/F12, or DMEM with 15μM hypoxanthine for 24 hours at 37 ℃ with 5% CO^2. For RNA isolation, coat the entire area of a 24-well culture plate with 500 μL of Bovine Collagen Coating Solution and incubate for 1 hour at 37 ℃ with 5% CO^2, then remove and immediately plate 3 x 10^4 cells/well in 500 μL of DMEM, DMEM/F12 or DMEM treated with 15μM hypoxanthine for 24 hours at 37 ℃ with 5% CO^2.

Mice

All animal experiments were conducted according to the University of Tsukuba guidelines for animal care and use. Two sets of oligonucleotides were annealed and inserted at the BbsI site of the pX459 (plasmid #48139; Addgene) to generate Cas9/sgRNA expression vectors. For the 5′ border: 5′ -caccgCTCTTCTTGCGGTCACGTTC-3′ and 5′ -aaacGAACGTGACCGCAAGAAGAGCc-3′ ; (overhanging nucleotides are shown in lowercase letters). Tail DNA from founder offspring was screened by PCR and sequencing.

Synapse formation assay

P21 wild type and FAT3 KO mice tissue sections were stained with the following antibodies against pre- and post-synaptic marker protein pairs: VGlut1 and PSD95 (excitatory), and GAD65 and Gephyrin (inhibitory). High magnification 63x objective images were obtained using a confocal laser scanning fluorescence microscopy (LSM700). The number of co-localized synaptic puncta of excitatory and inhibitory were obtained using the ImageJ plugin Puncta Analyzer (written by Bary Wark).

Statistical analysis

All experiments were performed in at least two independent experiments. All statistically compared data were analyzed by Student's *t*-test and one-way ANOVA by using GraphPad Prism (GraphPad Software). The statistical analyses of qRT-PCR are shown in Table 1.

RESULTS

FAT3 regulates BV2 morphology

To understand the mechanisms of how microglial morphology is controlled, I cultured microglial cell line BV2 with either a standard medium, DMEM or a high nutrient medium, DMEM/F12. When BV2 were cultured in DMEM, most cells exhibited round shape. On the other hand, when cells were cultured in DMEM/F12, the number of elongated cells was increased (Fig. 1A to 1C), indicating that microglial morphology is influenced by the surrounding culture condition.

Next, I explored the specific genes regulating BV2 morphogenesis under DMEM/F12 conditions. To investigate this, I conducted a microarray analysis. The global gene expression patterns were different for each condition. Some genes were significantly upregulated under DMEM/F12 (Fig. 2A). Although I found several interesting targets at least in this screening, one of the most interesting candidates is Fat3 gene. Because FAT3 has been reported to regulate neuronal morphology in retinal amacrine cells (Deans et al., 2011) (Krol et al., 2016), I presumed that FAT3 also controls the microglial morphogenesis. To confirm this idea, I surveyed FAT3 expression in microglia using the Brain RNA-seq database (http://www.brainrnaseq.org/). Interestingly, FAT3 expression is augmented in correlation with the timing of microglial transition around P14 (Fig. 2B), suggesting that FAT3 is a potential candidate, which controls microglial morphogenesis. I next investigated whether FAT3 expression in BV2 cells is affected by culture condition. FAT3 expression was upregulated when BV2 cells were cultured in DMEM/F12 (Fig. 2C). Particularly, it seems likely that DMEM/F12 facilitates FAT3 clustering in a distal process and a leading edge of lamellipodia. Also, FAT3 showed polarized localization in the cell body (Fig. 3A and 3B), demonstrating that the unknown specific factor in DMEM/F12 promotes FAT3 expression at the specific sites. I next investigated whether FAT3 is necessary for regulating their morphology through RNAi suppression. To do this, I first checked the efficiency of FAT3 siRNA. Treatment with siRNA significantly reduced DMEM/F12-induced expression levels of mRNA and changed immunostaining patters in BV2 cells (Fig. 4A and 4B). Using this siRNA, I examined the necessity of FAT3 for regulating morphogenesis. I found that FAT3 siRNA significantly suppressed the morphological changes even in DMEM/F12 culture conditions (Fig. 4C to 4E), suggesting that FAT3 regulates BV2 morphology depending on the culture condition.

Hypoxanthine promotes FAT3 expression in BV2 cells

I next investigated which factors in DMEM/F12 are implicated in inducing FAT3 expression in BV2 cells. To examine this, I divided the specific components of DMEM/F12, which are not included in DMEM, into three groups (i.e., non-essential amino acids, metallic ions, the others) (Fig. 5A), treated BV2 with them, and quantified the amount of FAT3 mRNA. When BV2 were cultured with DMEM/F12, FAT3 expression was clearly enhanced. However, DMEM containing either "non-essential amino acids" or "metallic ions" has little effect on the expression of FAT3. On the other hand, treatment of BV2 cells with "the others" enhanced FAT3 expression (Fig. 5B), indicating that the specific factor contained in "the others" is required for the FAT3 expression. Next, I surveyed which factors in "the others" regulate BV2 morphology. To answer this question, I additionally divided "the others" into 5 factors (i.e. hypoxanthine, biotin, vitamin B12, linoleic acid, and lipoic acid) and treated the cells with these compounds individually. Accordingly, treatment with hypoxanthine clearly induced FAT3 expression; however, other factors such as biotin, vitamin B12, linoleic acid, and lipoic acid did not have significant influences on the induction of FAT3 expression (Fig. 5C). Moreover, hypoxanthine stimulation enhances expression of FAT3 as well as DMEM/F12 culture conditions (Fig. 6A). Subsequently, to examine whether hypoxanthine is sufficient for the morphological changes of BV2, I analyzed the elongated shape of BV2 cells in the presence or absence of hypoxanthine. BV2 morphology exhibited elongated shape in the DMEM containing hypoxanthine (Fig. 6B to 6D). To further confirm whether hypoxanthine enhances FAT3 expression in microglia, I purified the primary microglia from neonatal mice. Treatment with hypoxanthine increased FAT3 expression in primary microglia, as well as BV2 cells (Fig. 7A and 7B). These data suggest that hypoxanthine is a key mediator that induces FAT3 expression in microglia.

Intracellular hypoxanthine is crucial for BV2 morphological changes

It has been known that P2X purinergic receptors play important role in microglial functions. Then, I investigated whether P2X purinergic receptor is a target of extracellular hypoxanthine using P2X purinergic receptor antagonist, PPADS (Fig. 8). Consequently, PPADS did not significantly block hypoxanthine-induced morphological changes of BV2 (Fig. 9A to 9C), implying that the P2X purinergic receptors have little effect on BV2 morphological changes depending on extracellular hypoxanthine. Because incubation with either DMEM/F12 or hypoxanthine slightly increased a concentration of intracellular hypoxanthine (Fig. 10A), I investigated whether intracellular hypoxanthine regulates microglial morphology. It has been reported that treatment with an

equilibrative nucleoside transporter (ENT) inhibitor, dipyridamole, is capable of increasing intracellular hypoxanthine via blocking export of hypoxanthine (Redies et al., 2012) (Fig. 8). Thus, I confirmed whether dipyridamole enhances a concentration of intracellular hypoxanthine in BV2 cells. I find that dipyridamole application slightly but significantly increased the hypoxanthine in BV2 cells (Fig. 10B). Using this condition, I quantified the BV2 morphology. The elongated BV2 cells were increased after the treatment with dipyridamole (Fig. 10C to 10E), implying that the intracellular concentration of hypoxanthine has an influence on BV2 morphology. To further confirm this, I used another inhibitor, allopurinol, which is a xanthine oxidase inhibitor (Fig. 11A). Since the xanthine oxidase is known to catalyze hypoxanthine to xanthine, inhibiting this enzyme also accumulates hypoxanthine in cells (Fig. 8). As I expected, treatment with allopurinol increased the elongated shape of BV2 cells (Fig. 11B to 11D). Taken together, these data suggest that upregulation of intracellular hypoxanthine promotes morphological changes of BV2 cells.

Hypoxanthine controls the BV2 morphological dynamics by a humoral factor

Microglial morphology is highly dynamic even in the resting state (Nimmerjahn et al., 2005). Since FAT3 is expressed at the timing of microglial transition (Bennett et al., 2016), I expected that my findings provide potential clues that underlie their morphological changes during postnatal stages. Then, I investigated the mechanisms by which BV2 shapes were changed over time using live-cell imaging analyses (Fig. 12A to 12C). The morphological changes of BV2 were highly dynamic and constantly shuttle between round and elongated shapes. Interestingly, BV2 cultured in DMEM including hypoxanthine slightly but significantly prolonged the retention time of elongated forms, suggesting that a potential function of FAT3 maintains elongated shapes and inhibits their retraction.

I next investigated the mechanisms of how BV2 shape is stabilized in the presence of hypoxanthine. Since a number of elongated BV2 were observed in a low-density cultured with DMEM/F12, I speculate that BV2 morphology is regulated by not only a cell-cell interaction but also a humoral factor, which is a potential ligand for FAT3. To answer this question, I cultured BV2 cells with or without the replacements of the medium. Consistent with my findings in Fig.1, both hypoxanthine and DMEM/F12 promoted the morphological changes. On the other hand, the number of the round shape of BV2 was increased even in the DMEM/F12 condition or DMEM containing hypoxanthine when the medium was exchanged frequently (Fig. 13A to 13D). At least in this condition, an adequate amount of FAT3 was expressed when cells were incubated with DMEM/F12 for 24 hours. Therefore, hypoxanthine induced FAT3 expression is not sufficient for altering BV2

DISCUSSION

In this study, I propose that the atypical cadherin family protein, FAT3, is a novel mediator that controls the morphology of microglia cell line BV2. I also found that hypoxanthine induces FAT3 expression. Moreover, FAT3 in concert with a potential humoral factor suppresses the retraction of BV2 processes. Thus, it is likely that hypoxanthine-Fat3 axis is crucial for regulating the microglial morphogenesis (Fig. 18).

In the nervous systems, cadherin family proteins, including FAT-related protein, play important roles in regulating a variety of neuronal aspects, including neuron-glia interaction, synaptogenesis, axon patterning, and dendritic arborization (Takeichi, 2007). So far, it has been shown that FAT3 and FAT1 are thought to be involved in actin rearrangement through interacting with ENA/VASP (Moller et al., 2004) (Tanoue and Takeichi, 2004) (Krol et al., 2016). Interestingly, FAT3 subcellular localization is not uniform but limited in a specific site. For instance, FAT3 has been reported to be asymmetrically localized to the processes in the inner plexiform layer in retinal amacrine cell precursors. The opposite processes of amacrine cells are retracted, resulting in forming unipolar cells (Deans et al., 2011) (Krol et al., 2016). In accordance with this research, I found that FAT3 in microglia is necessary for maintaining the processes in BV2 cells (Fig. 12A to 12C). Moreover, I also found that FAT3 subcellular localization is not diffusive at the peripheral region but concentrated locally. Therefore, I considered that asymmetric FAT3 localization anchors actin-related protein such as ENA/VASP and control the actin rearrangement under the FAT3-expressed region. As FAT-related proteins contribute homo- or heterophilic cell adhesion (Nakayama et al., 2002) (Ishiuchi et al., 2009), FAT3 target protein may have influences on the cell-cell contact or actin organization. So far, it has been reported that *Drosophila* Fat protein interacts with another cadherin family protein Dachsous (Ds), contributing to the regulation of planar cell polarity (Matakatsu and Blair, 2004). Intriguingly, the functions of both Fat and Ds are regulated by Four-jointed, which phosphorylates the Fat and Ds in the Golgi apparatus (Ishikawa et al., 2008). I found that expression of FAM20C, which is a secretary kinase as well as Four-jointed, is also increased when BV2 cells are cultured under DMEM/F12 medium (Fig. 1C). Therefore, it may be possible that a high nutrient condition could promote expressions of not only FAT3 but also FAM20C, leading to enhancing the interaction between FAT3 and target cadherin via FAT3 phosphorylation. Meanwhile, I found that the humoral factors secreted from BV2 cells have influences on their morphogenesis (Fig. 15A to 15D). Since proteomic analyses had revealed that FAT3 is associated with several humoral factors,

such as XCL1 and PDGFB (Huttlin et al., 2017), the FAT3-dependent morphogenesis is regulated by not only cell-cell interaction but also other extracellular proteins.

Although several purinergic receptors exist in microglia, I consider that microglial morphology relies on intracellular hypoxanthine for the following reasons: First, P0 purinergic receptors do not recognize hypoxanthine (Bender et al., 2002). Second, treatment with PPADS, which is an antagonist for P2X receptors, had little effect on changing BV2 morphology. Third, increasing intracellular hypoxanthine induces morphological changes of BV2. An important question is how hypoxanthine mediates FAT3 expression. It has been known that hypoxanthine mediates salvage pathways to synthesize nucleotides. Hypoxanthine-guanine phosphoribosyl transferase (HPRT1), which catalyzes hypoxanthine to inosine monophosphate (IMP) is one of the key enzymes that regulate the salvage pathway. Previously, HPRT1 expression level has been reported to be changed in microglia around P14 (Bennett et al., 2016). The proteomics analyses have revealed that HPRT1 interacts with several transcription factors, such as Jun and NF-κB (Li et al., 2015). Thus, it could be possible that hypoxanthine regulated HPRT1 cooperates with these transcription factors and upregulates FAT3 expression. Intriguingly, mutations in Hprt1 gene cause Lesch-Nyhan syndrome (LNS) (Yang et al., 1984), which is a rare neurological disorder exhibiting accumulation of uric acid caused by a defect in nucleic acid metabolism. Because a decrease of uric acid accumulation does not cure the LNS symptoms, aberrant microglial functions could be another possibility that abnormal hypoxanthine metabolism causes neurological disorders. The salvage pathway, rather than the *de novo* pathway, functions preferentially in the adulthood brain. On the other hand, it seems that the *de novo* pathway is activated dominantly under the postnatal stage, indicating that the switching from the *de novo* to the salvage pathways could occur after birth. Given that the upregulation of intracellular hypoxanthine concentration promotes HPRT1 activity, HPRT1 activation could be a key event that triggers the microglial transition under postnatal brains. Thus, it may be possible that loss of HPRT1 function causes the aberrant microglial transition, resulting in the onset of neuropsychiatric disorders, such as LNS.

BV2 cells are often used to be in place of primary microglia in an *in vitro* experiment because the gene expression patterns in BV2 cells are similar to the primary microglia under the reactive state (Henn et al., 2009). In addition, the analyses of BV2 cells have contributed to understanding the molecular mechanisms of intra- and inter-cellular phenomena, such as caspase signaling dependent microglia activation (Burguillos et al., 2011), the microglia and glioblastoma communication (Shen et al., 2016), and microglial phagocytosis (Pluvinage et al., 2019). Moreover,

BV2 cells are utilized to facilitate investigating the mechanisms of the neuronal disorder, such as Alzheimer's disease, Huntington's disease, amyotrophic lateral sclerosis and stroke (Urushitani et al., 2006) (Burguillos et al., 2015) (Zhao et al., 2018) (Joshi et al., 2019) (Pluvinage et al., 2019), indicating that BV2 cells are powerful tool to study the microglial functions. On the other hand, the shape of surveillant microglia *in vivo* is different from in BV2 cells.

FAT3 has been reported to be localized at the process in retinal amacrine cells and suppresses their retraction. Since FAT3 interacts with ENA/VASP protein, it is likely that FAT3 regulates a local actin reorganization in neurons. As well as amacrine cells, I found that treatment with hypoxanthine stabilizes their morphology in BV2 cells. Thus, I presume that one of FAT3 function is to control actin rearrangement and stabilize processes locally. The interesting questions is how subcellular localization of FAT3 is regulated. Since FAT3 is a cadherin family protein, the target expressed in other cells could influence on subcellular localization of microglial FAT3. Although this is an interesting enigma, a detailed analysis will be a need in the future.

The present study suggests that FAT3 is also expressed at the synapses of neurons and may be a novel communication signal between microglia and neurons. CD47-SIRPa was reported as a system to establish precise synaptic connectivity by neurons and microglia (Lehrman et al., 2018). Neuron-expressed CD47 is recognized by SIRPa, which is expressed on the microglial side and functions as a "don't eat me" signal to avoid synaptic pruning. Since FAT3 is localized at the synapses of neurons, this suggests that microglia may recognize the ligand for FAT3 that is presented at the synapse. Fat3-deficient mice had a reduced number of synapses, suggesting that FAT3 may be a novel "don't eat me" signal between neurons and microglia. The ligands of FAT3 are not yet known, but have been reported to bind homophilically in FAT2, the homolog of FAT3. In the FAT family, FAT2 is a homophilic binding and FAT4 binds heterophilically with Dachsous1(Nakayama et al., 2002) (Ishiuchi et al., 2009). These studies also suggest that cadherin binding to each other as well as the possibility of recognizing humoral factors.

In conclusion, I found that FAT3 regulates BV2 morphology in coordination with a humoral factor derived from BV2 cells. The amount of FAT3 in BV2 is regulated by intracellular hypoxanthine, demonstrating that the hypoxanthine-FAT3 axis is a novel pathway that links microglial morphogenesis to their traits. Since defects in FAT3 gene are associated with several neuropsychiatric diseases, such as schizophrenia, autism, and ataxia (Yan et al., 2016) (Baron et al., 2019) (Capkova et al., 2019), my finding may provide a hint that links microglial misregulations to the onset of these diseases.

ACKNOWLEDGMENTS

I express my deep thanks to Assistant professor Fuminori Tsuruta, Professor Tomoki Chiba and Assistant Professor Ban Sato (University of Tsukuba) for their persistent mentoring and guidance throughout this research. I was honored to work with them, and all other members of my laboratory, who provided helpful discussions and technical supports.

I also thank Dr. Hitomi Matsuzaki and Dr. Keiji Tanimoto (Tsukuba Advanced Research Alliance (TARA), University of Tsukuba) for supporting to generate the FAT3 deficient mice by CRISPR/Cas9 system and Dr. Yoshinori Kanemori, Dr. Shin-ichi Kashiwabara and Dr. Tadashi Baba (University of Tsukuba) for teaching me how to product anti-FAT3 antibodies.

FIGURES & TABLES

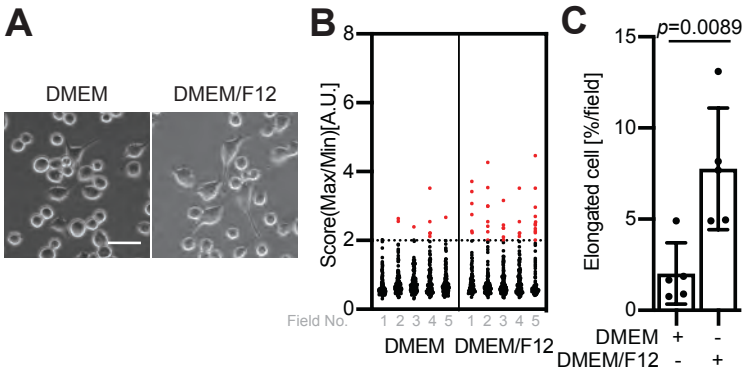

Figure 1. DMEM/F12 culture conditions induce elongation of protrusions in BV-2 cells

(A) BV2 cells were incubated with either DMEM as control medium or high nutrient medium, DMEM/F12 for 24 h. Scale bar represents 50μm. (B) Quantification of data from A. The score indicates a ratio of maximum to minimum Feret diameter (n > 78 cells, 5 field). The threshold of the elongated cells was defined by setting over 2. (C) The graph shows the relative percentage of the positive cells in each field. (n=5 field, Mean ± SD, p value was calculated by Student's t-test. The data were reproduced in at least five independent experiments).

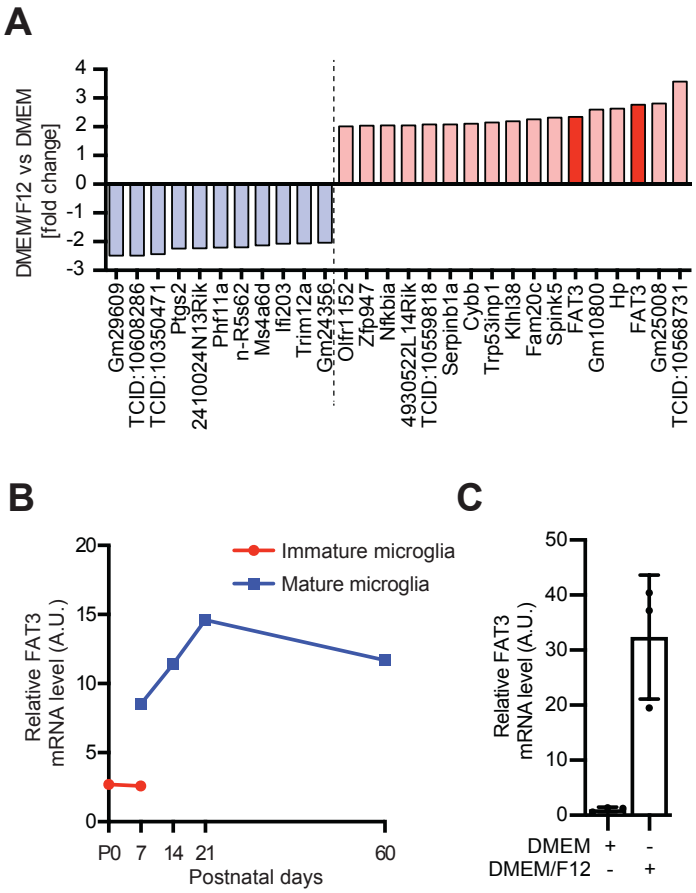

Figure 2. FAT3 is up-regulated in BV-2 cells cultured with DMEM/F12

(A) A subset of mRNAs identified in microarray experiments. The graph indicates the top 17 of upregulated and 11 of downregulated genes under DMEM/F12 culture condition. (B) The graph indicates *in silico* analysis of microglial FAT3 expression. The values were obtained from the Brain RNA-Seq database (http://www.brainrnaseq.org/). The red line indicates immature microglia (Tmem119- cells) and the blue line indicates mature microglia (Tmem119+ cells). (C) BV2 cells were incubated with either DMEM/F12 or DMEM for 24 hours. FAT3 mRNAs were measured by quantitative RT-PCR analysis and normalized to 5S ribosomal RNA. Mean ± SD; The data were reproduced in at least four independent experiments.

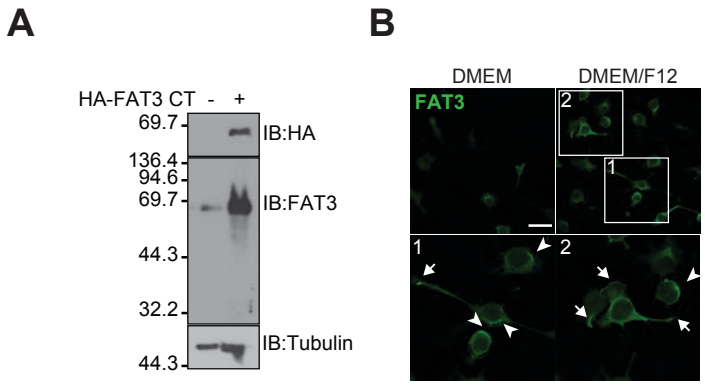

Figure 3. Anti-Fat3 antibody recognizes Fat3 on the projection of BV2.

(A) HEK293T cells were transfected with HA-FAT3 C-terminus (4313 - 4589) and subjected to immunoblot analysis with anti-FAT3, anti-HA, and anti-Tubulin antibodies. (B) Immunostaining showing the localization of FAT3 cultured in either DMEM or DMEM/F12. Arrow; FAT3 expression in the distal processes and lamellipodia. Arrowhead; FAT3 in the proximal region. Scale bar, 50 μm.

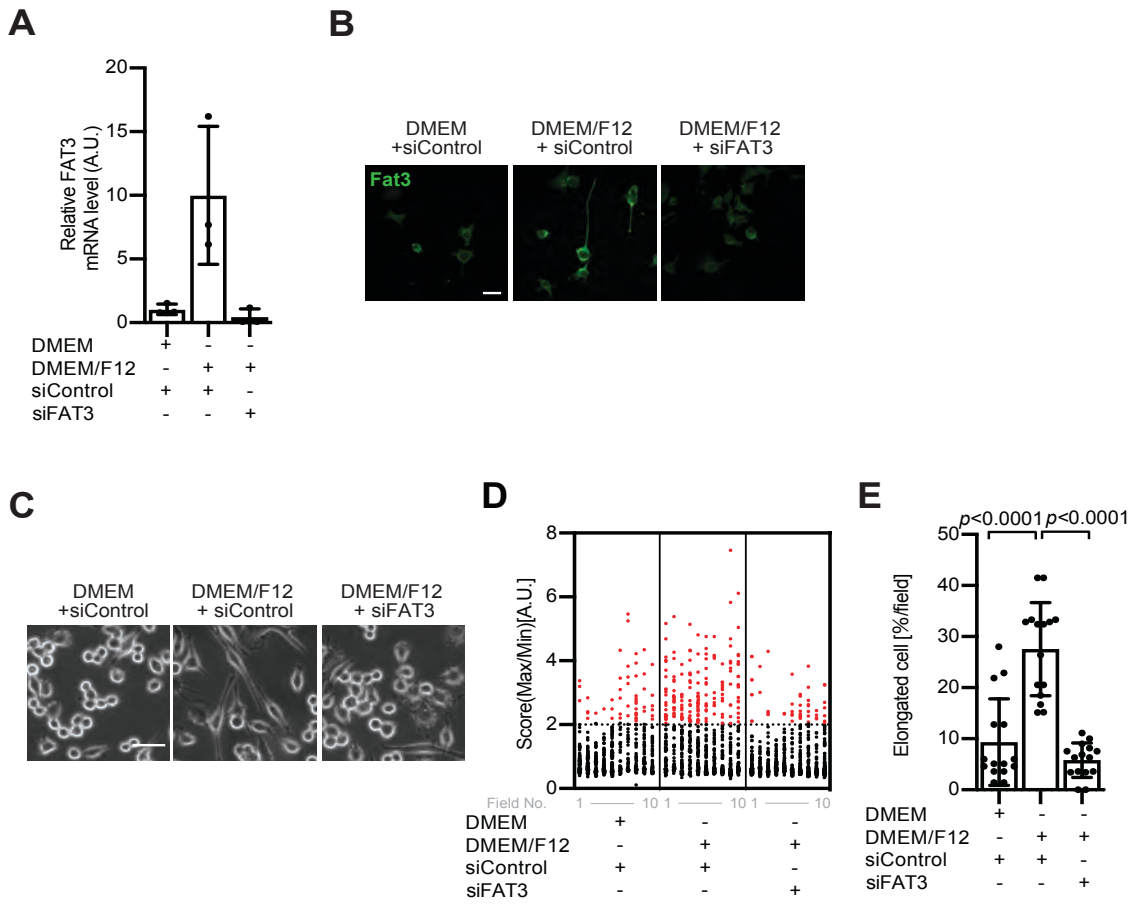

Figure 4. Inhibition of FAT3 expression reduces elongated cells

(A) BV2 cells were incubated for 24 hours after transfection of FAT3 siRNA. FAT3 mRNAs were measured by quantitative RT-PCR analysis and normalized to 5S ribosomal RNA. Mean ± SD; The data were reproduced in at least three independent experiments. (B) Immunostaining showing the FAT3 localization in the presence or absence of FAT3 siRNA for 24 hours. Scale bar, 50 µm. (C) BV2 cells were incubated in the presence or absence of FAT3 siRNA for 24 hours. Scale bar represents 50µm. (D) Quantification of data from C. The score indicates a ratio of maximum to minimum Feret diameter (n > 32 cells, 10 field). The threshold of the elongated cells was defined by setting over 2. (E) The graph shows the relative percentage of the positive cells in each field. (n=10 field, Mean ± SD, p value was calculated by one-way ANOVA. The data were reproduced in at least three independent experiments).

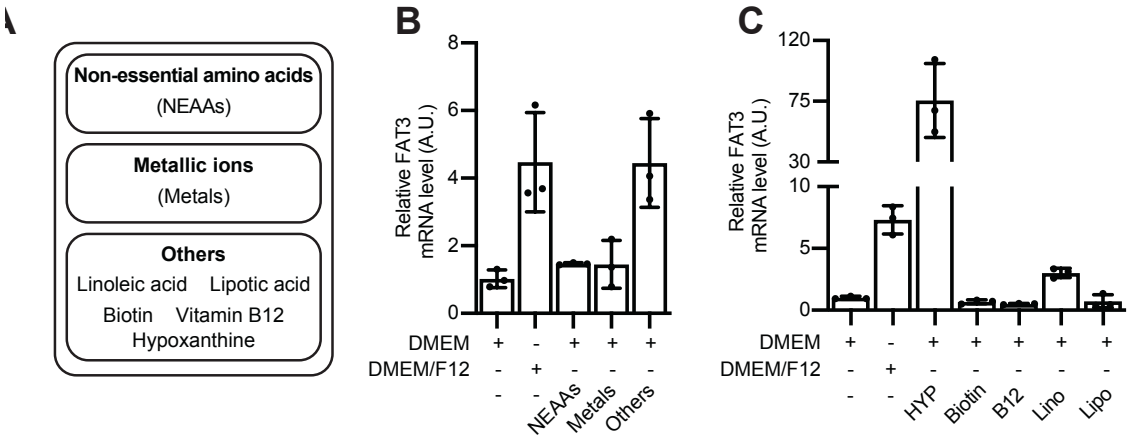

Figure 5. Hypoxanthine promotes FAT3 expression in BV2 cells

(A) The chart summarizes the DMEM/F12 components. They are categorized into three large groups, non-essential amino acids (NEAAs), metallic ions (metals) and Others. (B) BV2 cells were incubated with the indicated components for 24 hours. FAT3 mRNAs were measured by quantitative RT-PCR analysis and normalized to 5S ribosomal RNA. Mean ± SD, The data were reproduced in at least three independent experiments. (C) BV2 cells were incubated with either 15 μM hypoxanthine (HYP), 0.5 μM vitamin B12 (B12), 15 nM biotin, 0.15 μM linoleic acid (Lino) or 0.5 μM lipoic acid (Lipo), for 48 hours. The FAT3 mRNAs were measured by quantitative RT-PCR analysis and were normalized to 5S ribosomal RNA. Mean ± SD, The data were reproduced in at least four independent experiments.

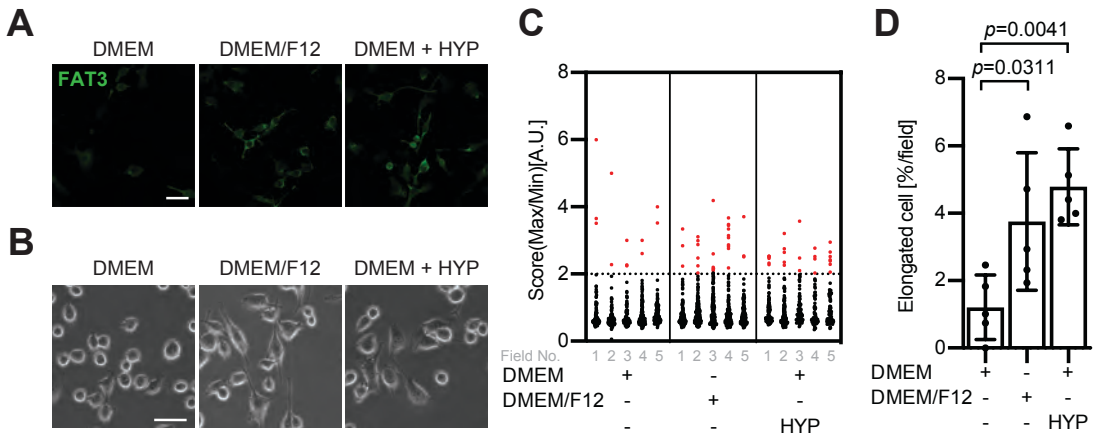

Figure 6. Hypoxanthine treatment elongates microglial protrusions via inducing FAT3 expression

(A) BV2 cells were incubated with either DMEM, DMEM/F12 or DMEM with 15 μM hypoxanthine for 24 hours. Immunostaining showing the FAT3 localization in the presence or absence of 15 μM hypoxanthine. Scale bar, 50 μm. (B) Phase contrast images showing BV2 morphology. Scale bar represents 50μm. (C) Quantification of data from B. The score indicates a ratio of maximum to minimum Feret diameter (n >68 cells, 5 field). The threshold of the elongated cells was defined by setting over 2. (D) The graph shows the relative percentage of the positive cells in each field. (n=5 field, Mean ± SD, p value was calculated by one-way ANOVA. The data were reproduced in at least four independent experiments).

2

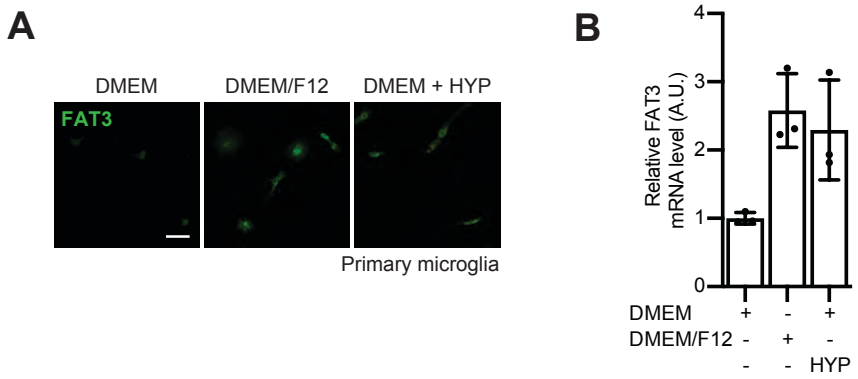

Figure 7. Hypoxanthine-induced FAT3 is upregulated in primary microglia

(A) The primary microglia were incubated with either DMEM, DMEM/F12 or DMEM with 15 μM hypoxanthine for 24 hours. Immunostaining showing the FAT3 expression in the presence or absence of 15 μM hypoxanthine. Scale bar, 50 μm. (B) The primary microglia were incubated with either DMEM, DMEM/F12 or DMEM with 15μM hypoxanthine for 24 hours. FAT3 mRNAs were measured by quantitative RT-PCR analysis and normalized to 5S ribosomal RNA. Mean ± SD, The data were reproduced in two independent experiments.

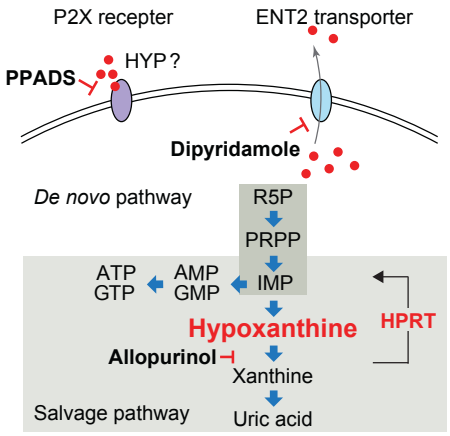

Figure 8. Schematic overview of purinergic metabolism

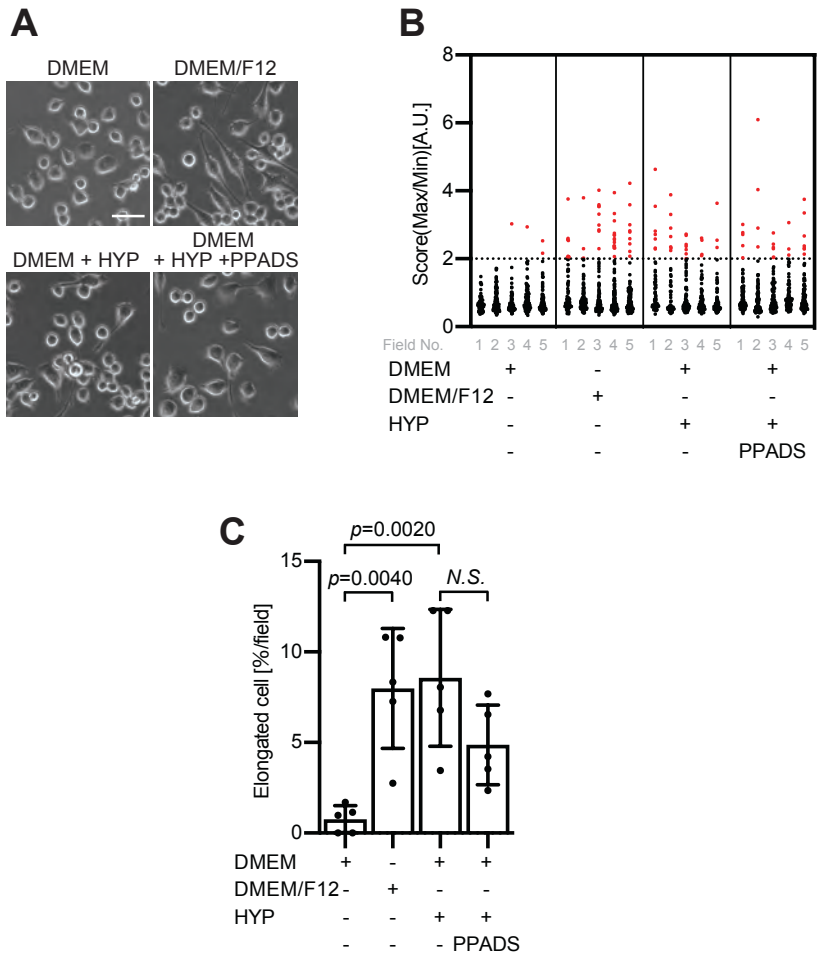

Figure 9. Inhibition of the P2X receptor does not affect the morphology of microglia

(A) BV2 cells were incubated in the presence or absence of 15 μM hypoxanthine and 100 μM PPADS for 24 hours. Scale bar represents 50 μm. The data were reproduced in at least three independent experiments. (B) Quantification of data from A. The score indicates a ratio of maximum to minimum Feret diameter (n >57 cells, 5 field). The threshold of the elongated cells was defined by setting over 2. (C) The graph indicates the relative percentage of elongated BV2 cells in C. Mean ± SD, p value was calculated by one-way ANOVA. N.S.; not significant

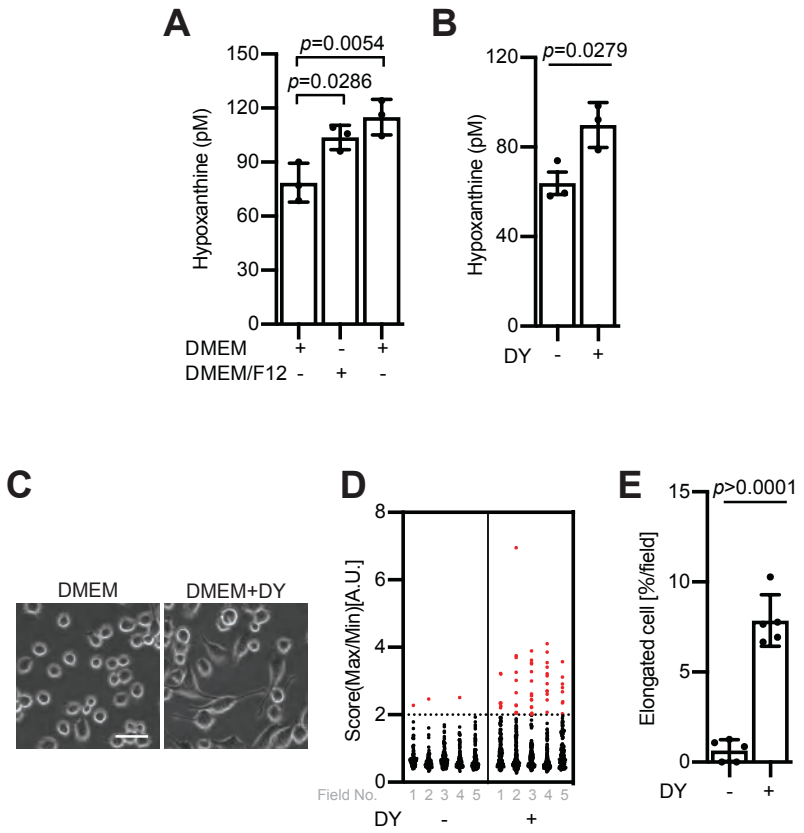

Figure 10. Dipyridamole increases intracellular hypoxanthine concentrations and affects the microglial morphology

(A) The graph indicates the intracellular hypoxanthine concentration cultured in DMEM/F12 or 15 μM hypoxanthine in DMEM for 3 hours. Mean ± SD, *p* value was calculated by one-way ANOVA. (B) The graph indicates the intracellular hypoxanthine concentration in the presence or absence of 10 μM dipyridamole (DY) cultured in DMEM for 3 hours. Mean ± SD, *p* value was calculated by Student's *t*-test. (C) BV2 cells were incubated in the presence or absence of 10 μM dipyridamole cultured in DMEM for 24 hours. Scale bar represents 50 μm. (D) Quantification of data from C. The score indicates a ratio of maximum to minimum Feret diameter (*n* >79 cells, 5 field). The threshold of the elongated cells was defined by setting over 2. (E) The graph indicates the relative percentage of elongated BV2 cells with or without dipyridamole in C. Mean ± SD, *p* value was calculated by Student's *t*-test. The data were reproduced in at least three independent experiments.

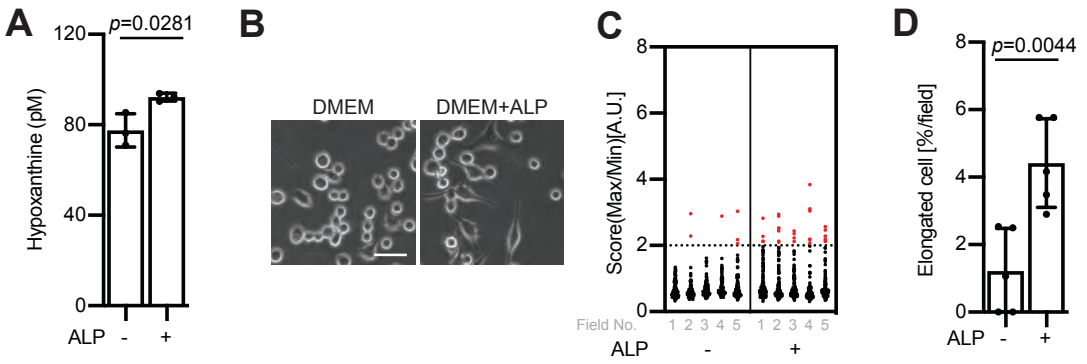

Figure 11. Inhibition of the intracellular hypoxanthine metabolic pathway increases microglial elongation cells

(A) The graph indicates the intracellular hypoxanthine concentration in the presence or absence of 10 μM allopurinol (ALP) cultured in DMEM for 3 hours. Mean ± SD, *p* value was calculated by Student's *t*-test. (B) BV2 cells were incubated in the presence or absence of 10 μM ALP cultured in DMEM for 24 hours. Scale bar represents 50 μm. (C) Quantification of data from B. The score indicates a ratio of maximum to minimum Feret diameter (n >79 cells, 5 field). The threshold of the elongated cells was defined by setting over 2. (D) The graph indicates the relative percentage of polarized BV2 cells in L. Mean ± SD, *p* value was calculated by Student's *t*-test. The data were reproduced in at least three independent experiments.

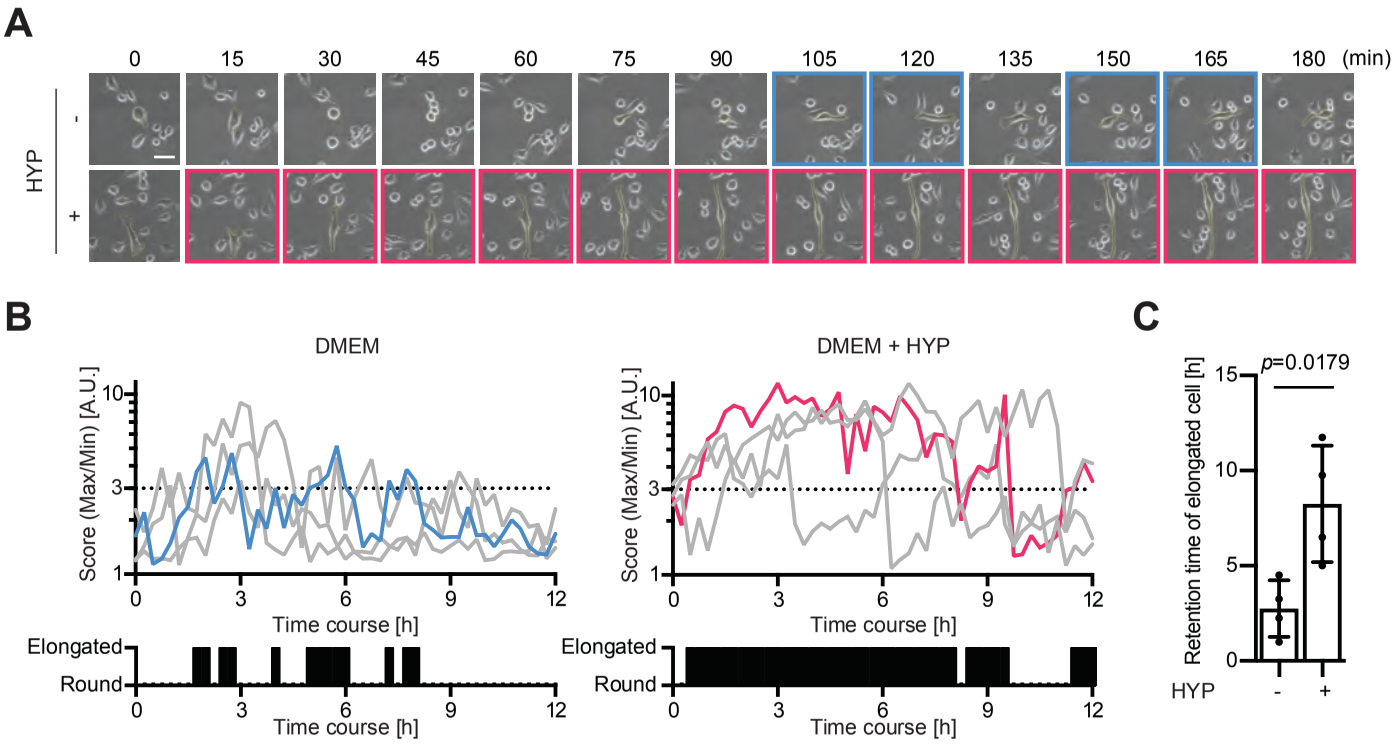

Figure 12. Hypoxanthine contributes to the stabilization of elongation of the protrusions

(A) BV2 cells were imaged at one frame per 15 minutes over for 12 hours with 1.0 μg/μL LPS in the presence or absence of hypoxanthine. Representative images are shown. The blue and red lines indicate the elongated cells. Scale bar indicates 20 μm. (B) The graph indicates the ratio of elongated shape by Feret's value. (C) The graph is summarized by data in B. Mean ± SD, *p* value was calculated by Student's *t*-test. The data were reproduced in at least three independent

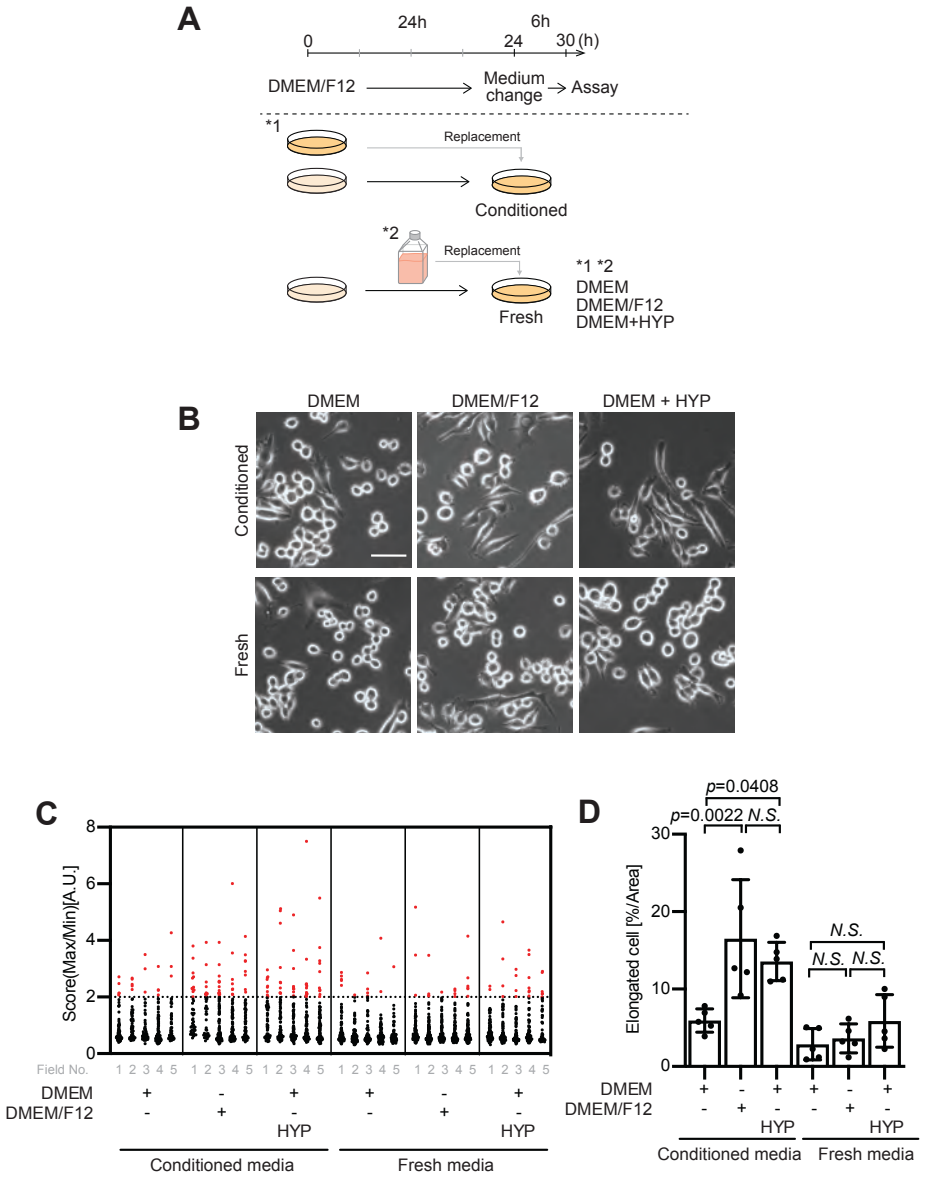

Figure 13. Hypoxanthine controls the morphology by a humoral factor

(A) Scheme of experiment. BV2 cells were incubated with DMEM/F12 medium for 24 hours and were then replaced with either conditioned or fresh media for 24 hours. For the conditioned media, other BV2 cells were incubated for 24 hours using indicated media. (B) Phase contrast images showing BV2 morphology. Scale bar indicates 50 µm. (C) The score indicates a ratio of maximum to minimum Feret diameter (n >39 cells, 5 field). The threshold of the elongated cells was defined by setting over 2. (D) The graph indicates the relative percentage of polarized BV2 cells morphology in E. Mean ± SD, p values were calculated by one-way ANOVA. N.S.; not significant. The data were reproduced in at least two independent experiments

.

BV-2 qPCR (Figure 2C)						
Unpaired *t* test	**Mean Diff.**	**95.00% CI of diff.**	**Significant?**	**Summary**	***p* value**	
DMEM vs. DMEM/F12	-4.973 ± 0.4619	-6.256 to -3.691	Yes	***	0.0004	

BV-2 siRNA qPCR (Figure 4A)						
Tukey's multiple comparisons test	**Mean Diff.**	**95.00% CI of diff.**	**Significant?**	**Summary**	**Adjusted *p* Value**	***p* value**
DMEM vs. DMEM/F12	3.192	-0.3346 to 6.718	No	ns	0.0719	A-B
DMEM vs. siFat3	-2.381	-5.907 to 1.146	No	ns	0.1763	A-C
DMEM/F12 vs. siFat3	-5.572	-9.099 to -2.046	Yes	**	0.0068	B-C

BV-2 NEAAs Metals Others qPCR (Figure 5B)							
Dunnett's multiple comparisons test	**Mean Diff.**	**95.00% CI of diff.**	**Significant?**	**Summary**	**Adjusted *p* Value**	**A-?**	
DMEM vs. DMEM/F12	2.113	1.032 to 3.195	Yes	***	0.0007	B	DMEM/F12
DMEM vs. NEAAs	0.5533	-0.5281 to 1.635	No	ns	0.4259	C	NEAAs
DMEM vs. Metals	0.4133	-0.6681 to 1.495	No	ns	0.6518	D	Metals
DMEM vs. Others	2.113	1.032 to 3.195	Yes	***	0.0007	E	Others

BV-2 Others qPCR (Figure 5C)							
Dunnett's multiple comparisons test	**Mean Diff.**	**95.00% CI of diff.**	**Significant?**	**Summary**	**Adjusted *p* Value**	**C-?**	
DMEM vs. DMEM/F12	2.858	1.779 to 3.936	Yes	****	<0.0001	A	DMEM/F12
DMEM vs. HYP	6.176	5.098 to 7.255	Yes	****	<0.0001	B	HYP
DMEM vs. Biotin	-0.5829	-1.661 to 0.4955	No	ns	0.4517	D	Biotin
DMEM vs. Linoleic	1.584	0.5057 to 2.663	Yes	**	0.0038	E	Linoleic
DMEM vs. VB12	-0.9733	-2.052 to 0.1052	No	ns	0.0839	F	VB12
DMEM vs. Lipoic	-0.6831	-1.761 to 0.3954	No	ns	0.3094	G	Lipoic

Primary micrglia qPCR (Figure 7B)							
Dunnett's multiple comparisons test	**Mean Diff.**	**95.00% CI of diff.**	**Significant?**	**Summary**	**Adjusted *p* Value**	**A-?**	
DMEM vs. DMEM/F12	1.35	0.629 to 2.06	Yes	**	0.003	B	DMEM/F12
DMEM vs. HYP	1.15	0.436 to 1.87	Yes	**	0.007	C	HYP

Table 1 qPCR statistical analysis

REFERENCES

Baron O, Grieshober D, Dias C, Fanto M (2019) Fat cadherins in mouse models of degenerative ataxias. Sci Rep 9:16155.

Bender E, Buist A, Jurzak M, Langlois X, Baggerman G, Verhasselt P, Ercken M, Guo HQ, Wintmolders C, Van den Wyngaert I, Van Oers I, Schoofs L, Luyten W (2002) Characterization of an orphan G protein-coupled receptor localized in the dorsal root ganglia reveals adenine as a signaling molecule. Proc Natl Acad Sci U S A 99:8573-8578.

Bennett ML, Bennett FC, Liddelow SA, Ajami B, Zamanian JL, Fernhoff NB, Mulinyawe SB, Bohlen CJ, Adil A, Tucker A, Weissman IL, Chang EF, Li G, Grant GA, Hayden Gephart MG, Barres BA (2016) New tools for studying microglia in the mouse and human CNS. Proc Natl Acad Sci U S A 113:E1738-1746.

Burguillos MA, Deierborg T, Kavanagh E, Persson A, Hajji N, Garcia-Quintanilla A, Cano J, Brundin P, Englund E, Venero JL, Joseph B (2011) Caspase signalling controls microglia activation and neurotoxicity. Nature 472:319-324.

Burguillos MA, Svensson M, Schulte T, Boza-Serrano A, Garcia-Quintanilla A, Kavanagh E, Santiago M, Viceconte N, Oliva-Martin MJ, Osman AM, Salomonsson E, Amar L, Persson A, Blomgren K, Achour A, Englund E, Leffler H, Venero JL, Joseph B, Deierborg T (2015) Microglia-Secreted Galectin-3 Acts as a Toll-like Receptor 4 Ligand and Contributes to Microglial Activation. Cell Rep 10:1626-1638.

Capkova P, Srovnal J, Capkova Z, Staffova K, Becvarova V, Trkova M, Adamova K, Santava A, Curtisova V, Hajduch M, Prochazka M (2019) MLPA is a practical and complementary alternative to CMA for diagnostic testing in patients with autism spectrum disorders and identifying new candidate CNVs associated with autism. PeerJ 6:e6183.

Cunningham CL, Martinez-Cerdeno V, Noctor SC (2013) Microglia regulate the number of neural precursor cells in the developing cerebral cortex. J Neurosci 33:4216-4233.

Deans MR, Krol A, Abraira VE, Copley CO, Tucker AF, Goodrich LV (2011) Control of neuronal morphology by the atypical cadherin Fat3. Neuron 71:820-832.

Fields RD, Burnstock G (2006) Purinergic signalling in neuron-glia interactions. Nat Rev Neurosci 7:423-436.

Filipello F et al. (2018) The Microglial Innate Immune Receptor TREM2 Is Required for Synapse

Elimination and Normal Brain Connectivity. Immunity 48:979-991.e978.

Gevi F, Zolla L, Gabriele S, Persico AM (2016) Urinary metabolomics of young Italian autistic children supports abnormal tryptophan and purine metabolism. Mol Autism 7:47.

Haynes SE, Hollopeter G, Yang G, Kurpius D, Dailey ME, Gan WB, Julius D (2006) The P2Y12 receptor regulates microglial activation by extracellular nucleotides. Nat Neurosci 9:1512-1519.

Henn A, Lund S, Hedtjarn M, Schrattenholz A, Porzgen P, Leist M (2009) The suitability of BV2 cells as alternative model system for primary microglia cultures or for animal experiments examining brain inflammation. ALTEX 26:83-94.

Hua JY, Smith SJ (2004) Neural activity and the dynamics of central nervous system development. Nat Neurosci 7:327-332.

Huttlin EL et al. (2017) Architecture of the human interactome defines protein communities and disease networks. Nature 545:505-509.

Ishikawa HO, Takeuchi H, Haltiwanger RS, Irvine KD (2008) Four-jointed is a Golgi kinase that phosphorylates a subset of cadherin domains. Science 321:401-404.

Ishiuchi T, Misaki K, Yonemura S, Takeichi M, Tanoue T (2009) Mammalian Fat and Dachsous cadherins regulate apical membrane organization in the embryonic cerebral cortex. J Cell Biol 185:959-967.

Joshi AU, Minhas PS, Liddelow SA, Haileselassie B, Andreasson KI, Dorn GW, 2nd, Mochly-Rosen D (2019) Fragmented mitochondria released from microglia trigger A1 astrocytic response and propagate inflammatory neurodegeneration. Nat Neurosci 22:1635-1648.

Kettenmann H, Hanisch UK, Noda M, Verkhratsky A (2011) Physiology of microglia. Physiol Rev 91:461-553.

Krol A, Henle SJ, Goodrich LV (2016) Fat3 and Ena/VASP proteins influence the emergence of asymmetric cell morphology in the developing retina. Development 143:2172-2182.

Lehrman EK, Wilton DK, Litvina EY, Welsh CA, Chang ST, Frouin A, Walker AJ, Heller MD, Umemori H, Chen C, Stevens B (2018) CD47 Protects Synapses from Excess Microglia-Mediated Pruning during Development. Neuron 100:120-134.e126.

Li X, Wang W, Wang J, Malovannaya A, Xi Y, Li W, Guerra R, Hawke DH, Qin J, Chen J (2015) Proteomic analyses reveal distinct chromatin-associated and soluble transcription factor complexes. Mol Syst Biol 11:775.

Lichtman JW, Colman H (2000) Synapse elimination and indelible memory. Neuron 25:269-278.

Marin-Teva JL, Dusart I, Colin C, Gervais A, van Rooijen N, Mallat M (2004) Microglia promote the death of developing Purkinje cells. Neuron 41:535-547.

Matakatsu H, Blair SS (2004) Interactions between Fat and Dachsous and the regulation of planar cell polarity in the Drosophila wing. Development 131:3785-3794.

Miyamoto A, Wake H, Ishikawa AW, Eto K, Shibata K, Murakoshi H, Koizumi S, Moorhouse AJ, Yoshimura Y, Nabekura J (2016) Microglia contact induces synapse formation in developing somatosensory cortex. Nat Commun 7:12540.

Moller M, Berg F, Riquet J, Pomp D, Archibald A, Anderson S, Feve K, Zhang Y, Rothschild M, Milan D, Andersson L, Tuggle CK (2004) High-resolution comparative mapping of pig Chromosome 4, emphasizing the FAT1 region. Mamm Genome 15:717-731.

Nagae S, Tanoue T, Takeichi M (2007) Temporal and spatial expression profiles of the Fat3 protein, a giant cadherin molecule, during mouse development. Dev Dyn 236:534-543.

Nakayama M, Nakajima D, Yoshimura R, Endo Y, Ohara O (2002) MEGF1/fat2 proteins containing extraordinarily large extracellular domains are localized to thin parallel fibers of cerebellar granule cells. Mol Cell Neurosci 20:563-578.

Nimmerjahn A, Kirchhoff F, Helmchen F (2005) Resting microglial cells are highly dynamic surveillants of brain parenchyma in vivo. Science 308:1314-1318.

Paolicelli RC, Bolasco G, Pagani F, Maggi L, Scianni M, Panzanelli P, Giustetto M, Ferreira TA, Guiducci E, Dumas L, Ragozzino D, Gross CT (2011) Synaptic pruning by microglia is necessary for normal brain development. Science 333:1456-1458.

Pluvinage JV, Haney MS, Smith BAH, Sun J, Iram T, Bonanno L, Li L, Lee DP, Morgens DW, Yang AC, Shuken SR, Gate D, Scott M, Khatri P, Luo J, Bertozzi CR, Bassik MC, Wyss-Coray T (2019) CD22 blockade restores homeostatic microglial phagocytosis in ageing brains. Nature 568:187-192.

Redies C, Hertel N, Hubner CA (2012) Cadherins and neuropsychiatric disorders. Brain Res 1470:130-144.

Saugstad OD (1988) Hypoxanthine as an indicator of hypoxia: its role in health and disease through free radical production. Pediatr Res 23:143-150.

Schafer DP, Lehrman EK, Kautzman AG, Koyama R, Mardinly AR, Yamasaki R, Ransohoff RM, Greenberg ME, Barres BA, Stevens B (2012) Microglia sculpt postnatal neural circuits in

an activity and complement-dependent manner. Neuron 74:691-705.

Shen X, Burguillos MA, Osman AM, Frijhoff J, Carrillo-Jimenez A, Kanatani S, Augsten M, Saidi D, Rodhe J, Kavanagh E, Rongvaux A, Rraklli V, Nyman U, Holmberg J, Ostman A, Flavell RA, Barragan A, Venero JL, Blomgren K, Joseph B (2016) Glioma-induced inhibition of caspase-3 in microglia promotes a tumor-supportive phenotype. Nat Immunol 17:1282-1290.

Sierra A, Encinas JM, Deudero JJ, Chancey JH, Enikolopov G, Overstreet-Wadiche LS, Tsirka SE, Maletic-Savatic M (2010) Microglia shape adult hippocampal neurogenesis through apoptosis-coupled phagocytosis. Cell Stem Cell 7:483-495.

Stevens B, Allen NJ, Vazquez LE, Howell GR, Christopherson KS, Nouri N, Micheva KD, Mehalow AK, Huberman AD, Stafford B, Sher A, Litke AM, Lambris JD, Smith SJ, John SW, Barres BA (2007) The classical complement cascade mediates CNS synapse elimination. Cell 131:1164-1178.

Takeichi M (2007) The cadherin superfamily in neuronal connections and interactions. Nat Rev Neurosci 8:11-20.

Tanoue T, Takeichi M (2004) Mammalian Fat1 cadherin regulates actin dynamics and cell-cell contact. J Cell Biol 165:517-528.

Ueno M, Fujita Y, Tanaka T, Nakamura Y, Kikuta J, Ishii M, Yamashita T (2013) Layer V cortical neurons require microglial support for survival during postnatal development. Nat Neurosci 16:543-551.

Urushitani M, Sik A, Sakurai T, Nukina N, Takahashi R, Julien JP (2006) Chromogranin-mediated secretion of mutant superoxide dismutase proteins linked to amyotrophic lateral sclerosis. Nat Neurosci 9:108-118.

Viktorinova I, Konig T, Schlichting K, Dahmann C (2009) The cadherin Fat2 is required for planar cell polarity in the Drosophila ovary. Development 136:4123-4132.

Yan P, Qiao X, Wu H, Yin F, Zhang J, Ji Y, Wei S, Lai J (2016) An Association Study Between Genetic Polymorphisms in Functional Regions of Five Genes and the Risk of Schizophrenia. J Mol Neurosci 59:366-375.

Yang TP, Patel PI, Chinault AC, Stout JT, Jackson LG, Hildebrand BM, Caskey CT (1984) Molecular evidence for new mutation at the hprt locus in Lesch-Nyhan patients. Nature 310:412-414.

Zhang Y, Chen K, Sloan SA, Bennett ML, Scholze AR, O'Keeffe S, Phatnani HP, Guarnieri P, Caneda C, Ruderisch N, Deng S, Liddelow SA, Zhang C, Daneman R, Maniatis T, Barres BA, Wu JQ (2014) An RNA-sequencing transcriptome and splicing database of glia, neurons, and vascular cells of the cerebral cortex. J Neurosci 34:11929-11947.

Zhao Y, Wu X, Li X, Jiang LL, Gui X, Liu Y, Sun Y, Zhu B, Pina-Crespo JC, Zhang M, Zhang N, Chen X, Bu G, An Z, Huang TY, Xu H (2018) TREM2 Is a Receptor for beta-Amyloid that Mediates Microglial Function. Neuron 97:1023-1031 e1027.